Published in final edited form as:
Cell Host Microbe. 2012 February 16; 11(2): 153–166. doi:10.1016/j.chom.2012.01.008.

Focal Adhesion Kinase Is a Component of Antiviral RIG-I-like Receptor Signaling

Rebecca A. Bozym[1], **Elizabeth Delorme-Axford**[1], **Katharine Harris**[1], **Setanie Morosky**[1], **Mine Ikizler**[2,4], **Terence S. Dermody**[2,3,4], **Saumendra N. Sarkar**[1,5], and **Carolyn B. Coyne**[1,*]

[1]Department of Microbiology and Molecular Genetics, Vanderbilt University School of Medicine, Nashville, Tennessee 37232

[2]Department of Pediatrics, Vanderbilt University School of Medicine, Nashville, Tennessee 37232

[3]Department of Pathology, Microbiology, and Immunology, Vanderbilt University School of Medicine, Nashville, Tennessee 37232

[4]Elizabeth B. Lamb Center for Pediatric Research, Vanderbilt University School of Medicine, Nashville, Tennessee 37232

[5]University of Pittsburgh Cancer Institute, University of Pittsburgh, Pittsburgh, Pennsylvania 15219, USA

SUMMARY

Viruses modulate the actin cytoskeleton at almost every step of their cellular journey, from entry to egress. Cellular sensing of these cytoskeletal changes may function in the recognition of viral infection. Here we show that focal adhesion kinase (FAK), a focal adhesion localized tyrosine kinase that transmits signals between the extracellular matrix and the cytoplasm, serves as a RIG-I-like receptor antiviral signaling component by directing mitochondrial antiviral signaling adaptor (MAVS) activation. Cells deficient in FAK are highly susceptible to RNA virus infection and attenuated in antiviral signaling. We show that FAK interacts with MAVS at the mitochondrial membrane in a virus infection-dependent manner and potentiates MAVS-mediated signaling via a kinase-independent mechanism. A cysteine protease encoded by enteroviruses cleaves FAK to suppress its role in innate immune signaling, These findings suggest that FAK serves as a link between cytoskeletal perturbations that occur during virus infection and activation of innate immune signaling.

*Address correspondence: Carolyn B. Coyne, 518 Bridgeside Point II, 450 Technology Drive, Pittsburgh, PA 15219, Phone (412) 383-5149, Fax (412) 624-1401, coynec2@pitt.edu.

INTRODUCTION

The induction of innate immune signaling is essential for host cell defense against viral infection. Retinoic acid inducible gene-I (RIG-I) and melanoma differentiation associated gene 5 (MDA5) are functionally related intracellular viral recognition molecules that recognize cytoplasmic dsRNA produced as a replication intermediate in the life cycle of many RNA viruses. Activated RIG-I and MDA5 converge on a common downstream adaptor molecule, mitochondrial antiviral signaling ([MAVS], also known as VISA/IPS-1/Cardif) that activates nuclear factor (NF)-κB and interferon (IFN) regulatory factor (IRF)-3/7 to regulate type I interferon (IFN) production (Kawai et al., 2005; Seth et al., 2005; Xu et al., 2005).

In addition to the innate immune system, host cells protect themselves from pathogen infection by physical barriers often supported by the actin cytoskeleton. Perturbations of the actin cytoskeleton by depolymerizing agents induce NF-κB- and IRF3-mediated signaling, and several components of immune signaling associate with the actin cytoskeleton (Kustermans et al., 2005; Legrand-Poels et al., 2007; Mukherjee et al., 2009; Nemeth et al., 2004). Focal adhesions (FAs) are the primary site at which cells adhere to the extracellular matrix and associate with the actin cytoskeleton. Focal adhesion kinase (FAK) is a protein tyrosine kinase located primarily at FAs that serves as a key component in the transmission of signals between the extracellular matrix and the cytoplasm. FAK contains a central kinase domain flanked by two large non-catalytic domains. The N-terminal region (referred to as the FERM domain due to its homology with band 4.1, ezrin, radixin, and moesin) regulates FAK activity, whereas the C-terminal domain contains a focal adhesion targeting (FAT) domain with binding sites for other proteins located at FAs such as paxillin, talin, and vinculin (Schaller, 2010). The clustering of integrins promotes FAK activation, resulting in the tyrosine phosphorylation of FAK at position 397 (Y397), an event that facilitates binding of Src family tyrosine kinases to this site and subsequent Src-mediated phosphorylation events, leading to maximal FAK activity. FAK is required for development, as deletion of FAK causes embryonic lethality (Braren et al., 2006; Shen et al., 2005).

In this study, we identify a role for FAK in the regulation of RIG-I-like receptor (RLR)-mediated type I IFN induction in response to RNA virus infections. We show that mouse embryonic fibroblasts (MEFs) deficient in FAK are highly susceptible to RNA virus infection and incapable of activating NF-κB signaling in response to RNA virus replication. In addition, $FAK^{-/-}$ MEFs are attenuated in the capacity to induce RIG-I- and MAVS-mediated IFNβ production. Furthermore, we found that FAK interacts with MAVS in a virus infection-dependent manner and potentiates MAVS-mediated signaling via a kinase-independent mechanism. We also show that coxsackievirus B (CVB), a member of the enterovirus family, directly cleaves FAK as a means to attenuate its antiviral signaling and that this cleavage is mediated by the virally-encoded $3C^{pro}$ cysteine protease. Cleavage of FAK by $3C^{pro}$ generates two distinct cleavage fragments. The C-terminal cleavage fragment functions as an FRNK-like polypeptide that acts as a dominant-negative inhibitor of FAK-mediated antiviral signaling. Taken together, these data show that FAK plays a role in host cell antiviral innate immune signaling and that CVB targets FAK as a mechanism to evade FAK-mediated type I IFN induction.

RESULTS

FAK Deficiency Enhances RNA Virus Replication and Impairs NF-κB and IFNβ Signaling

To determine whether FAK functions in antiviral innate immune signaling, we infected wild-type ($FAK^{+/+}$) or FAK-deficient ($FAK^{-/-}$) MEFs (Figure S1A) with a panel of RNA viruses including coxsackievirus B (CVB), vesicular stomatitis virus (VSV), reovirus (ReoV), or Sendai virus (SeV). In all cases, $FAK^{-/-}$ MEFs displayed a significant enhancement in susceptibility to virus replication as assessed by immunofluorescence microscopy (Figure 1A, 1B) and plaque assays (Figure 1C, 1D). This effect was specific for RNA viruses, as there were no significant differences in the replication of a DNA virus (vaccinia virus [VV]) in $FAK^{+/+}$ and $FAK^{-/-}$ MEFs (Figures 1A and S1C), and infection by another DNA virus, herpes simplex virus-1 (HSV-1), was reduced in $FAK^{-/-}$ MEFs (Figure 1B).

Because we found that FAK-deficient MEFs were highly sensitive to infection by diverse RNA viruses, we next determined whether $FAK^{-/-}$ MEFs were deficient in NF-κB activation or type I IFN induction in response to virus infection or RLR activation. We found that $FAK^{-/-}$ MEFs exhibited significantly reduced NF-κB promoter activity in response to SeV and VSV infection (Figure 1E). Likewise, we found that NF-κB activation was ablated in $FAK^{-/-}$ MEFs transfected with poly(I:C), a synthetic dsRNA ligand for RLR signaling (Figure 1E), and enhancement of IκBα mRNA expression in response to poly(I:C) was reduced in $FAK^{-/-}$ MEFs (Figure 1G). In contrast to NF-κB activation, $FAK^{-/-}$ MEFs were capable of activating IFNβ in response to SeV, VSV, and infection (Figure 1F). However, despite the significant enhancement of viral replication (and subsequent levels of dsRNA produced), we observed similar levels of IFNβ in $FAK^{+/+}$ and $FAK^{-/-}$ MEFs. Consistent with these findings, we found that there was a partial diminution of IFNβ induction in $FAK^{-/-}$ MEFs transfected with poly(I:C) (Figure 1F) and reduced upregulation of IFNβ mRNA levels in response to this treatment (Figure 1G). We also found that the relocalization of IRF3 to the nucleus in response to SeV infection was significantly reduced in $FAK^{-/-}$ MEFs compared with $FAK^{+/+}$ control MEFs (Figure S1D). These results show that FAK is required for NF-κB induction in response to RNA virus infection and functions in IRF3-mediated IFNβactivation.

To demonstrate that the absence of FAK was responsible for the attenuation of NF-κB and IFNβ activation in response to RLR engagement in $FAK^{-/-}$ MEFs, we expressed FAK in these cells and quantified NF-κB and IFNβ activation in response to poly(I:C) transfection. Expression of FAK in $FAK^{-/-}$ MEFs restored NF-κB signaling and enhanced IFNβ activation in response to poly(I:C) transfection (Figure 1H) and also inhibited virus replication (not shown), suggesting that these pathways are attenuated in the absence of FAK.

FAK Expression Enhances Antiviral Signaling in an Autophosphorylation-independent Manner

As we observed a role for FAK in antiviral signaling in MEFs, we next determined the consequences of FAK silencing and overexpression on NF-κB and IFNβ promoter activities

in human embryonic kidney (HEK) 293 cells. Downregulation of FAK by RNAi-mediated silencing led to a partial reduction of both NF-κB and IFNβ promoter activity in response to SeV infection (Figures 2A, 2B, and S2A). In contrast, FAK overexpression enhanced NF-κB promoter activity (Figure 2C) and IFNβ responses (Figure 2D) following SeV infection. Similar results were obtained using an ISRE luciferase reporter (Figure S2C) and by immunoblotting for ISG60 (Figure S2D).

The tyrosine kinase activity of FAK is induced by autophosphorylation of Y397. To assess the role of FAK kinase activity in antiviral signaling, we altered this residue (FAK^{Y397F}) and determined the effect of this mutation on NF-κB and IFNβ activity in response to SeV infection. Overexpression of autophosphorylation-deficient FAK (FAK^{Y397F}) promoted SeV-induced NF-κB and IFNβ activation to a greater extent than wild-type FAK, suggesting that phosphorylation of this residue serves as a negative regulator of FAK-mediated antiviral signaling (Figure 2C, 2D).

FAK signaling is negatively regulated by expression of a FAK variant containing the C-terminal noncatalytic domain, termed FAK-related nonkinase (FRNK), which is autonomously or selectively expressed in several cell types (Nolan et al., 1999) and functions as a dominant-negative inhibitor of FAK (Richardson and Parsons, 1996). We found that expression of FRNK partially inhibited SeV-induced NF-κB and IFNβ signaling (Figure 2E, 2F). However, expression of the FERM domain of FAK alone had no significant effect on SeV-induced NF-κB or IFNβ signaling compared with vector controls (Figure 2E, 2F). These results suggest that the localization of FAK to FAs is required for its participation in antiviral signaling and that FRNK expression acts in a dominant-negative manner to attenuate FAK-mediated innate immune signaling.

Induction of type I IFN signaling upregulates the expression of genes associated with antiviral signaling. We found that overexpression of RIG-I and MAVS, but not a mutant form of RIG-I incapable of inducing type I IFN signaling (RIG-I ΔN), in HEK293 cells induced a enhancement of endogenous FAK expression (Figure S2E). Moreover, incubation of cells with purified IFNβ (100 U) was sufficient to induce FAK upregulation (Figure S2E). The FAK promoter contains several NF-κB binding sites (Golubovskaya et al., 2004), and our analysis revealed the presence of several consensus ISRE and STAT1 binding sites (not shown).

FAK Is Involved in MAVS-mediated Antiviral Signaling

As we observed that $FAK^{-/-}$ MEFs are deficient in NF-κB activation and partially attenuated in IFNβ activation in response to RNA virus infection and that FAK overexpression is sufficient to upregulate NF-κB and IFNβ signaling in HEK293 cells, we next determined whether FAK antiviral signaling occurs upstream or downstream of RIG-I and MAVS. Whereas NF-κB was significantly activated in $FAK^{+/+}$ MEFs by expression of a constitutively active mutant of RIG-I (RIG-I ΔC) or wild-type MAVS, expression of either construct in $FAK^{-/-}$ MEFs failed to elicit substantial changes in NF-κB induction (Figure 3A). In contrast, expression of TRAF6, which signals downstream of activated MAVS, elicited NF-κB activation in both $FAK^{+/+}$ and $FAK^{-/-}$ MEFs, although the induction was at least partially attenuated in $FAK^{-/-}$ MEFs (Figure 3A).

Consistent with our findings on IFNβ induction in $FAK^{-/-}$ MEFs in response to virus infection (Figure 1D), we found that IFNβ activity was partially abrogated in $FAK^{-/-}$ MEFs in response to RIG-I ΔC and MAVS overexpression (Figure 3B). Similar results were obtained using an ISRE luciferase reporter (Figure S2F). This inhibition occurred downstream of MAVS, as expression of a constitutively active mutant of IRF3 (IRF3-5D) or expression of IKKε elicited IFNβ signaling to comparable levels in $FAK^{+/+}$ and $FAK^{-/-}$ MEFs (Figure 3B). Taken together, these findings indicate that FAK is required for MAVS-mediated NF-κB activation and suggest that it may also function in MAVS-mediated IFNβ induction.

FAK Interacts with MAVS following Virus Infection and Redistributes to Mitochondria

Our findings thus far demonstrate that FAK plays an important role in innate immune signaling in response to RNA virus infection at a step in the pathway likely downstream of MAVS. Consistent with this model, we found that enhancement of IFNβ promoter activity in HEK293 cells overexpressing FAK was abolished in cells transfected with MAVS siRNA (Figures 3C and S2B). Furthermore, overexpressed MAVS upregulated NF-κB and IFNβ activation in response to SeV infection to a substantially greater extent in the presence of overexpressed FAK (Figure 3D and 3E). FAK-mediated upregulation of MAVS antiviral signaling was further enhanced by coexpression of MAVS with FAK^{Y397F}, further suggesting that phosphorylation at this site acts as a negative regulator of innate immune signaling (not shown).

The activation of antiviral RLR signaling induces the formation of a protein complex enriched in components associated with innate immune signaling. We found that FAK co-immunoprecipitated with MAVS and components of MAVS-mediated signaling such as RIP1 and TRAF3 in a manner dependent on SeV infection (Figure 3F). In contrast, we did not observe interactions between FAK and RIG-I or STING, another RLR-associated adaptor molecule (Ishikawa and Barber, 2008), and we did not detect association between FAK and the TLR3 adaptor, TRIF (Figure 3F). To confirm an interaction between FAK and MAVS we performed *in vitro* binding assays using recombinant Flag-MAVS and overexpressed HA-tagged FAK immunopreciitated from HEK293 lysates and found that FAK and MAVS interacted using this approach (Figure 3G).

Because MAVS is localizes to the mitochondrial membrane, whereas FAK is enriched at FAs, we next investigated the localization of FAK in the absence or presence of viral infection by immunofluorescence microscopy. In uninfected cells, FAK was localized to FAs, but MAVS was almost exclusively associated with mitochondria (Figure 3H). Following infection of cells with SeV, we observed significant redistribution of FAK from FAs to the mitochondrial membrane, where it colocalized with MAVS (Figure 3H). We also found that FAK^{Y397F} both coimmunoprecipitated and colocalized with MAVS, even in the absence of virus infection, indicating that the relocalization of FAK and its association with MAVS does not require its kinase activity (Figure S3A, S3B).

To identify the domain of MAVS that interacts with FAK, we expressed N-terminal (1-148 aa) or C-terminal (149-540 aa) MAVS fragments and performed coimmunoprecipitation experiments with overexpressed FAK. We found that the N-terminal domain of MAVS was

sufficient to interact with FAK, although it appeared to do so with less efficiency than full-length MAVS (Figure 3I), suggesting that MAVS localization to mitochondria mediates its interaction with FAK. Thus, our data indicate that following virus infection, FAK is recruited to the mitochondrial membrane where it forms an association with the N-terminal domain of MAVS to enhance NF-κB- and IFNβ-mediated antiviral signaling.

MAVS Relocalization in Response to Virus Infection Involves FAK

Virus infection induces the aggregation of MAVS, which is an essential step in the activation of RLR-mediated antiviral signaling (Hou et al., 2011; Onoguchi et al., 2010). To determine whether FAK is involved in MAVS reorganization or whether MAVS reorganization is compromised in the absence of FAK, we investigated the localization of EGFP-MAVS in $FAK^{+/+}$ and $FAK^{-/-}$ MEFs. In uninfected $FAK^{+/+}$ MEFs, MAVS colocalized with the mitochondria (Figure 4A, 4B, left). Following infection with VSV (Figure 4A) or SeV (Figure 4B), MAVS relocalized into large cytoplasmic aggregates, consistent with the relocalization of MAVS observed by others (Hou et al., 2011; Onoguchi et al., 2010). In $FAK^{-/-}$ MEFs, MAVS exhibited an abnormal pattern of localization even in uninfected cells that consisted of large clusters within the cytoplasm that remained unchanged in response to virus infection (Figure 4A, 4B, right). Quantification of MAVS-associated mitochondrial length revealed that mitochondrial morphology differed significantly in uninfected $FAK^{+/+}$ and $FAK^{-/-}$ MEFs and supported the dramatic relocalization of MAVS into small, punctate structures following virus infection of $FAK^{+/+}$ MEFs (Figure 4C). We found that expression of wild-type FAK in $FAK^{-/-}$ MEFs restored normal MAVS localization and mitochondrial morphology (Figure 4D). Taken together, these data suggest that FAK participates in some aspect of MAVS localization and that MAVS signaling is compromised due in part to this mislocalization.

CVB Infection Elicits FAK Redistribution and Cleavage

Viruses commonly target central components of RLR signaling as a means to antagonize cell-intrinsic immunity. We found that infection with CVB, a member of the enterovirus family of RNA viruses, led to dramatic rearrangements of the actin cytoskeleton associated with loss of stress fibers, disassembly of FAs, and redistribution of FAK from FAs to the cytoplasm (Figure S4A). In addition to a marked pattern of relocalization, CVB infection also was associated with the appearance of a FAK cleavage fragment (Figure 5A). Whereas full-length FAK migrated as a single band of ~ 125 kD in uninfected cells, we detected a distinct FAK cleavage fragment migrating at ~ 100 kD using an N-terminal-directed FAK antibody in cells infected with CVB (Figure 5A). In contrast, CVB infection did not induce any alterations in the migration pattern of other FA-associated components such as paxillin, talin, or vinculin (Bozym et al., 2011). The kinetics of FAK cleavage were consistent with enhanced viral replication, as FAK cleavage was evident by 4-5 hr post-infection (p.i.), which corresponded with the appearance of newly replicated CVB, cleavage of eIF4G1, shutdown of host protein synthesis, and production of nascent viral RNA (Figure S4B, S4C, S4D).

CVB 3C^{pro} Cleaves FAK

Enteroviruses encode specific proteases that process the viral polyprotein, but which also target a variety of host molecules. We found that expression of the CVB 3C^{pro} cysteine protease was sufficient to induce many of the alterations in the actin cytoskeleton observed during CVB infection including a loss of stress fibers and breakdown of FAs as well as inducing the relocalization of FAK from FAs (Figure S4E). As neither CVB infection nor 3C^{pro} expression leads to cleavage of vinculin or other FA-associated components [(Bozym et al., 2011) and not shown] these findings suggest that loss of FAK association with FAs induces widespread effects on many FA-associated components. We also found that expression of 3C^{pro} induced a significant loss of endogenous FAK expression and the appearance of a ~ 100 kD N-terminal cleavage fragment (Figure 5B). The relocalization and cleavage of FAK by 3C^{pro} required its cysteine protease activity, as cotransfection of a catalytically inactive 3C^{pro} mutant (C147A) (Lee et al., 2009) had no effect on FAK localization (Figure S4E) or expression (Figure 5B).

To identify the extent of FAK cleavage by 3C^{pro}, we constructed a FAK expression construct containing an HA-epitope tag at the N-terminus and a Flag-epitope tag at the C-terminus. Expression of wild-type, but not catalytically inactive, 3C^{pro} induced the appearance of two distinct FAK cleavage fragments, an HA-positive fragment migrating at ~ 100 kD and a much smaller Flag-positive fragment of ~ 25 kD (Figure 5C). Interestingly, we found that the HA- and Flag-containing fragments of FAK exhibited marked differences in their pattern of subcellular localization in the presence of 3C^{pro}. The C-terminal Flag-containing fragment of FAK remained associated with FAs, whereas the N-terminal fragment exhibited diffuse localization within the cytoplasm (Figure 5D). Taken together, these data point to a role for 3C^{pro} in the cleavage of FAK during CVB infection and suggest that 3C^{pro} cleavage generates two distinct fragments of FAK.

3C^{pro} Cleaves FAK at a Single Site within its C-terminal Domain

CVB 3C^{pro} preferentially cleaves glutamine-glycine (Q-G) bonds in both the viral polyprotein and cellular targets (Blom et al., 1996). Sequence analysis revealed that FAK contains a consensus 3C^{pro} cleavage site located within the C-terminus at position Q852 (Figure 5E, top). Cleavage at this site is anticipated to produce cleavage fragments of ~ 100 kD and ~ 25 kD, which are consistent with the size of the fragments in CVB-infected and 3C^{pro}-transfected cells (Figure 5A, 5B, 5C). We engineered a site-directed mutant of this residue (Q852A) to determine whether it served as the primary 3C^{pro} cleavage site. We found that Q852A-FAK was resistant to 3C^{pro}-mediated cleavage, whereas expression of 3C^{pro} with wild-type FAK generated an ~ 100 kD N-terminal cleavage fragment (Figure 5E, bottom). Similarly, whereas the N-terminus of FAK was redistributed from FAs to the cytoplasm, mutant Q852A FAK retained its FA localization in the presence of 3C^{pro} expression and displayed very little cytoplasmic localization (Figure S4F). We also found that FA length and protein composition (as assessed by vinculin immunolocalization) was compromised in cells expressing wild-type FAK and 3C^{pro}, whereas cells expressing Q852A FAK retained FA length and vinculin localization (Figure S4F). Therefore, 3C^{pro} cleaves FAK at a single site (Q852) within its C-terminal domain.

3C^{pro}-mediated FAK Cleavage Fragments Exhibit Differential Localization

We next determined whether either of the possible 3C^{pro}-induced cleavage fragments of FAK remain functionally active and retain proper cellular localization. We constructed EGFP-fused expression constructs of the N-terminal (NT fragment, residues 1-852) or C-terminal (CT fragment, residues 853-1052) fragments of FAK that would result from 3C^{pro} cleavage (Figure 5F, top). We found that the NT fragment of FAK (1-852) no longer localized to FAs and was instead distributed almost exclusively within the cytoplasm (Figure 6A). In contrast, the CT fragment of FAK (853-1052) retained FA localization similar to wild-type FAK (Figure 6A). The differential localization of the NT and CT fragments of FAK are consistent with our studies using dual NT HA-tagged and CT Flag-tagged FAK in the presence of 3C^{pro} (Figure 5D).

The CT 3C^{pro} Cleavage Fragment of FAK Functions as an FRNK-like Polypeptide

As the CT cleavage fragment of FAK generated by 3C^{pro} cleavage is similar in size and composition to FRNK (Figure 6B), we determined whether this fragment negatively regulates FAK function. We found that expression of the CT fragment of FAK induced a dramatic decrease in the level of phosphotyrosine (pTyr)-containing proteins concentrated at FAs (Figure 6B) and potently inhibited cell migration (Figure 6C), properties associated with FRNK expression (Chan et al., 2011; Richardson and Parsons, 1996). Collectively, these data suggest that 3C^{pro}-mediated cleavage of FAK generates a CT cleavage fragment that functions to suppress FA-associated signaling and cell migration.

In addition to its prominent role in cell migration and adhesion, FAK is involved in NF-κB-dependent cell survival in response to TNFα, which can be inhibited by FRNK expression (Funakoshi-Tago et al., 2003; Huang et al., 2007; Zhang et al., 2006). We found that expression of the CT fragment of FAK acted as a dominant-negative inhibitor of wild-type FAK- and NT fragment-mediated induction of NF-κB and repressed NF-κB activation under both resting and TNFα-exposed conditions (Figure 6E).

3C^{pro} Cleavage Fragments of FAK Bind MAVS and Suppress Antiviral Signaling

Because we found that the CT fragment of FAK inhibited FAK-dependent NF-κB signaling in response to TNFα, we next determined whether this fragment might also attenuate MAVS-mediated antiviral signaling. We found that both the NT and CT FAK cleavage fragments co-immunoprecipitated with MAVS from SeV-infected cells (Figure 7A) and that the CT FAK fragment was relocalized from FAs to sites of MAVS localization in response to SeV infection (Figure 7B). In addition, whereas expression of FAK upregulated NF-κB and IFNβ activation in the presence of overexpressed MAVS, expression of both the NT and CT fragments of FAK led to a partial inhibition of SeV-induced MAVS signaling, particularly with respect to the induction of type I IFNs (Figure 7C, 7D). Consistent with a role for the NT and CT fragments of FAK in attenuating MAVS-mediated antiviral signaling, we found that expression of the NT and CT cleavage fragments of FAK enhanced VSV replication when overexpressed in HEK293 cells (Figure 7E), and expression of the Q852A non-cleavable mutant of FAK significantly inhibited CVB replication (Figure 7F). Taken together, these data show that the cleavage of FAK induced by 3C^{pro} generates two

dominant-negative fragments and that both the N-terminal and C-terminal domains of FAK are required to fully stimulate MAVS signaling.

DISCUSSION

Here we report on the finding that FAK functions in MAVS-mediated antiviral signaling and is targeted by the virally-encoded $3C^{pro}$ protease of CVB as a means to suppress innate immune signaling. Moreover, we show that the $3C^{pro}$-generated cleavage fragments of FAK function as dominant-negative inhibitors of FAK-mediated MAVS signaling, indicating that CVB uses a highly specific strategy to inhibit FAK as a means to evade host innate immunity.

Although our data implicate FAK as an important regulator of MAVS, its precise function in regulating RLR signaling remains unclear. We found that mutation of a key phosphorylation site in FAK did not inhibit MAVS-mediated signaling but instead led to further induction of the antiviral response. Consistent with this finding, we did not observe tyrosine phosphorylation of MAVS in cells overexpressing FAK in the absence or presence of viral infection (not shown). In addition to its role as a tyrosine kinase, FAK serves as a scaffolding molecule in a variety of signaling cascades by virtue of its FERM and FAT domains and multiple proline-rich recognition motifs. Thus, the intracellular localization of FAK may allow it to function as a scaffold in a variety of cellular processes. We observed the redistribution of FAK to the mitochondrial membrane where it colocalized with MAVS, suggesting that FAK localization is a fundamental aspect of its control of MAVS signaling. Interestingly, the tyrosine phosphorylation of FAK at Y397 acts as an important determinant of FAK localization to FAs and correlates with an enhancement of FAK localization to those sites (Hamadi et al., 2005). Thus, our data showing that mutation of this residue further potentiates MAVS signaling is consistent with a model in which FAK relocalization from FAs to MAVS acts as an important switch to enhance antiviral innate immune responses, likely by facilitating its role as a scaffold to enhance RLR signaling.

The spatiotemporal localization of MAVS is an important aspect of its function in innate immune signaling. RIG-I activation induces the aggregation of MAVS into detergent-insoluble fractions that form prion-like fibrils (Hou et al., 2011). Virus infection leads to the redistribution of MAVS (Onoguchi et al., 2010), and MAVS localization to mitochondrial-ER membrane synapses is required to promote RIG-I signaling (Horner et al., 2011). The formation of MAVS aggregates serves to recruit components involved in MAVS-mediated NF-κB and IRF3 induction and is thus a necessary component of RLR signaling. We found that FAK-deficient MEFs were completely attenuated in the capacity to activate MAVS-mediated NF-κB signaling and at least partially attenuated in the capacity to activate MAVS-mediated type I IFN induction. Furthermore, we found that MAVS exhibited an abnormal pattern of cellular localization in FAK-deficient MEFs. Whereas MAVS localized in a classical mitochondrial filamentous pattern in $FAK^{+/+}$ MEFs, it localized with mitochondria in a cluster-like pattern in $FAK^{-/-}$ MEFs. Mitochondria are capable of altering their shape and cellular localization in response to various stimuli. Mitochondrial morphology is influenced by the actin cytoskeleton, and a variety of actin cytoskeletal-associated components play key roles in mitochondrial structure and function (Boldogh and

Pon, 2007). Therefore, the reorganization of the mitochondrial membrane that accompanies MAVS-mediated innate immune signaling may require components associated with the actin cytoskeleton. Our data suggest that FAK couples actin cytoskeletal changes to the alterations in mitochondrial morphology that accompany MAVS-mediated innate immune signaling. Although the precise cellular mechanism by which FAK facilitates MAVS localization is not known, it is likely that FAK functions as a scaffold to recruit the signaling and cytoskeletal components to the mitochondrial membrane required for MAVS relocalization.

The actin cytoskeleton is an important component of innate immune signaling in plants, which rely strictly on innate immune signaling for pathogen defense by a strategy referred to as the 'guard hypothesis.' In this model, plant innate immune signaling is not solely governed by the recognition of pathogen associated molecular patterns (PAMPs) but is also induced indirectly (via the activation of 'R proteins') by the cellular changes induced by pathogen effectors that function to suppress or alter antimicrobial signaling (Jones and Dangl, 2006). The actin cytoskeleton acts as a platform for R protein-mediated innate immune signaling in plants, and the function of several R proteins depends on an intact actin network (Tian et al., 2009; Wang et al., 2009). Our data suggest that components of the actin cytoskeleton may play similar roles in the mammalian innate immune system and direct the redistribution of innate immune-associated components necessary to initiate signaling, act as scaffolding molecules to bridge components of the innate immune system, or function as sensors for modulation of the actin cytoskeleton by microbial pathogens that lead to antimicrobial signal induction.

As it is unlikely that FAK participates in detection of PAMPs, what induces FAK to participate in antiviral signaling and relocalize from FAs to sites of MAVS localization? FAs provide an important structural link between the cell and the extracellular matrix and are primed to detect even subtle alterations in the actin cytoskeleton and respond to these changes with the induction of intracellular signaling. Thus, components associated with FAs have the capacity to detect microbial pathogens, which often disassemble or modulate the actin cytoskeleton during their entry, replication, or egress. Changes in the actin cytoskeleton induced by virus infection may alter the phosphorylation state of FAK and/or its association with FAs, thus rendering the molecule more accessible to bind MAVS at the mitochondrial membrane. The association between FAK and MAVS thus might prime the host cell for the induction of PAMP-mediated signaling and serve to augment the antiviral response.

Targeted proteolysis of molecules associated with innate immune pathways serves as a powerful means to eliminate antiviral signaling. Although the cleavage of FAK by CVB might facilitate the breakdown of the actin cytoskeleton that accompanies enteroviral infections, our data suggest that the targeted proteolysis of FAK by $3C^{pro}$ is a strategy employed by the virus to evade MAVS-mediated antiviral signaling. We found that cleavage of FAK by $3C^{pro}$ inactivates the protein and generates two fragments that function in a dominant-negative capacity to suppress MAVS signaling. Both the NT and CT fragments of FAK predicted to be generated by $3C^{pro}$ cleavage have the capacity to suppress MAVS-mediated NF-κB and IFNβ induction. Although we have shown that $3C^{pro}$ also cleaves

MAVS (Mukherjee et al., 2011), the cleavage of FAK (and other components associated with RLR signaling) would serve to add an additional layer of protection by which the virus evades host innate immunity. It is likely that other viral pathogens also target FAK as a means of innate immune evasion. Such evasion could be accomplished via the direct cleavage of FAK by virally-encoded proteases (such as occurs with CVB) or modulation of FAK signaling as a means to sequester FAK at FAs where it would be incapable of potentiating MAVS signaling.

FAK is localized predominantly to FAs, where it is primed to respond to subtle changes in the actin cytoskeleton and induce intracellular signaling in response to these changes. Our findings indicate that FAK also functions in MAVS-mediated NF-κB and type I IFN signaling in response to viral infections and that it is targeted by virally-encoded protease as a means to attenuate its antiviral signaling. A better understanding of the mechanisms employed by FAK to modulate antiviral signaling in response to virus infections and how these processes are attenuated by viruses will yield insights into the regulation of innate immune responses by actin cytoskeletal-associated components.

EXPERIMENTAL PROCEDURES

Cells and Virus

HEK293 cells and human osteosarcoma U2OS cells were cultured in DMEM-H supplemented to contain 10% FBS and 1x penicillin/streptomycin. $FAK^{+/+}$ and $FAK^{-/-}$ MEFs were provided by Jun-Lin Guan (University of Michigan, Ann Arbor, MI) and maintained in DMEM-H supplemented to contain 10% FBS and 1x penicillin/streptomycin.

Experiments were performed with CVB3-RD (expanded as previously described [Coyne and Bergelson, 2006]), recombinant GFP-expressing vesicular stomatitis virus (VSV, as described (Zhu et al., 2011), Sendai virus (SeV, Cantell strain purchased from Charles River Laboratories), reovirus (ReoV, T3 Dearing strain), GFP-tagged herpes simplex virus-1 (HSV1, strain KOS, provided by Fred Homa and previously described (Desai and Person, 1998), or GFP-tagged vaccinia virus (VV, previously described (Moser et al., 2010). Experiments quantifying productive virus infection were performed with the indicated viral inocula for the indicated times. Plaque assays were conducted using MEF (VSV) or HeLa (CVB) cells as indicated. Confluent monolayers were adsorbed with serial dilutions of virus for 2 hr at 37°C (VSV) or 1 hr at room temperature (CVB), after which the cells were overlayed with agarose and incubated for 48 hr. Plaques were visualized following crystal violet staining and enumerated.

Immunoblots

Cells were grown in 6-well or 24-well plates, and lysates were prepared with RIPA buffer (50 mM Tris-HCl [pH 7.4], 1% NP-40, 0.25% sodium deoxycholate, 150 mM NaCl, 1 mM EDTA, 1mM phenylmethanesulfonyl fluoride, 1 mg/ml aprotinin, leupeptin, and pepstatin). Lysates were loaded into wells of 4-20% Tris-HCl gels (Bio-Rad, Hercules, CA) and transferred to polyvinylidene difluoride membranes. Membranes were blocked using 5% nonfat dry milk, probed with the indicated antibodies, and developed using horseradish

peroxidase-conjugated secondary antibodies (Santa Cruz Biotechnology) and SuperSignal West Pico or Dura chemiluminescent substrates (Pierce Biotechnology).

In some cases, immunoblots were analyzed using an Odyssey Infrared Imaging System (LI-COR Biosciences). Whole-cell lysates from transfected cells (30 μg) were loaded into wells of 4–20% Tris-HCl gels, separated electrophoretically, and transferred to nitrocellulose membranes. Membranes were blocked using Odyssey Blocking Buffer and incubated with the appropriate antibodies overnight at 4°C in Odyssey Blocking Buffer. Following washing, membranes were incubated with anti-rabbit or anti-mouse antibodies conjugated to IRDye 680 or 800CW in the presence of 0.02% SDS and visualized using the Odyssey Infrared Imaging System according to the manufacturer's instructions.

Reporter Gene Assay

Activation of the NF-κB and IFNβ promoter was quantified using a reporter-gene assay. Cells were transfected in 24-well plates with p-125 luc (IFNβ) or NF-κB reporter plasmid together with the indicated plasmids. Luciferase activity was measured by the Dual-Luciferase assay kit (Promega) using a Synergy 2 luminescence plate reader (Bio-Tek). Poly(I:C) complexed to transfection reagent LyoVec was purchased from Invivogen, and non-complexed poly(I:C) was purchased from GE Healthcare Life Sciences. Data are expressed as fold induction over mock-infected or vector-transfected controls. All experiments were performed in triplicate and conducted a minimum of three times.

Immunofluorescence microscopy

Monolayers grown in collagen-coated chamber slides (BD Biosciences, San Jose, CA) were fixed in 4% PFA, washed in PBS containing 50 mM NH_4Cl for 5 min, and permeabilized with 0.1% Triton X-100 in PBS. Cells were incubated with the indicated primary antibodies for 1 h at RT, washed, and incubated with Alexa Fluor-conjugated secondary antibodies. Following washing, cells were fixed and mounted with Vectashield containing DAPI and images captured using an Olympus IX81 inverted microscope equipped with a motorized *Z*-axis drive and deconvolved using a calculated point-spread function (Slidebook 5.0) or with a FV1000 Olympus confocal laser scanning microscope. Quantification of focal adhesion length, phosphotyrosine content within FAs, and mitochondria lengths were measured and quantified using Olympus FV10-ASW software (version 02.01b). At least 100 FAs or mitochondrial fibrils were measured per cell for a total of at least 30 cells per condition.

Statistical Analysis

Data are presented as mean ± standard deviation. One-way analysis of variance (ANOVA) and Bonferroni's correction for multiple comparisons were used to determine statistical significance ($P \leq 0.05$ or ≤ 0.001).

Supplementary Material

Refer to Web version on PubMed Central for supplementary material.

Acknowledgments

We thank Jun-Lin Guan for generously providing us with the HA-FAK expression construct and $FAK^{+/+}$ and $FAK^{-/-}$ MEFs, Fred Homa for GFP-HSV1, and Jeff Bergelson for careful review of the manuscript. This research was supported by Public Health Service awards R01 AI081759 (C.B.C.) and R37 AI038296 (T.S.D.) and the Elizabeth B. Lamb Center for Pediatric Research. Additional support was provided by Public Health Service awards CA68485 for the Vanderbilt-Ingram Cancer Center and DK20593 for the Vanderbilt Diabetes Research and Training Center.

Literature cited

Blom N, Hansen J, Blaas D, Brunak S. Cleavage site analysis in picornaviral polyproteins: discovering cellular targets by neural networks. Protein Sci. 1996; 5:2203–2216. [PubMed: 8931139]

Boldogh IR, Pon LA. Mitochondria on the move. Trends Cell Biol. 2007; 17:502–510. [PubMed: 17804238]

Bozym, RA.; Patel, K.; White, C.; Cheung, KH.; Bergelson, JM.; Morosky, SA.; Coyne, CB. Calcium signals and Calpain-dependent Necrosis are essential for Release of Coxsackievirus B from Polarized Intestinal Epithelial Cells.. Mol Biol Cell. 2011.

Braren R, Hu H, Kim YH, Beggs HE, Reichardt LF, Wang R. Endothelial FAK is essential for vascular network stability, cell survival, and lamellipodial formation. J Cell Biol. 2006; 172:151–162. [PubMed: 16391003]

Chan KT, Bennin DA, Huttenlocher A. Regulation of adhesion dynamics by calpain-mediated proteolysis of focal adhesion kinase (FAK). J Biol Chem. 2011; 285:11418–11426. [PubMed: 20150423]

Desai P, Person S. Incorporation of the green fluorescent protein into the herpes simplex virus type 1 capsid. Journal of virology. 1998; 72:7563–7568. [PubMed: 9696854]

Funakoshi-Tago M, Sonoda Y, Tanaka S, Hashimoto K, Tago K, Tominaga S, Kasahara T. Tumor necrosis factor-induced nuclear factor kappaB activation is impaired in focal adhesion kinase-deficient fibroblasts. J Biol Chem. 2003; 278:29359–29365. [PubMed: 12748169]

Golubovskaya V, Kaur A, Cance W. Cloning and characterization of the promoter region of human focal adhesion kinase gene: nuclear factor kappa B and p53 binding sites. Biochimica et biophysica acta. 2004; 1678:111–125. [PubMed: 15157737]

Hamadi A, Bouali M, Dontenwill M, Stoeckel H, Takeda K, Ronde P. Regulation of focal adhesion dynamics and disassembly by phosphorylation of FAK at tyrosine 397. J Cell Sci. 2005; 118:4415–4425. [PubMed: 16159962]

Horner, SM.; Liu, HM.; Park, HS.; Briley, J.; Gale, M, Jr.. Mitochondrial-associated endoplasmic reticulum membranes (MAM) form innate immune synapses and are targeted by hepatitis C virus.. Proc Natl Acad Sci U S A. 2011.

Hou F, Sun L, Zheng H, Skaug B, Jiang QX, Chen ZJ. MAVS Forms Functional Prion-like Aggregates to Activate and Propagate Antiviral Innate Immune Response. Cell. 2011; 146:448–461. [PubMed: 21782231]

Huang D, Khoe M, Befekadu M, Chung S, Takata Y, Ilic D, Bryer-Ash M. Focal adhesion kinase mediates cell survival via NF-kappaB and ERK signaling pathways. Am J Physiol Cell Physiol. 2007; 292:C1339–1352. [PubMed: 17135301]

Ishikawa H, Barber GN. STING is an endoplasmic reticulum adaptor that facilitates innate immune signalling. Nature. 2008; 455:674–678. [PubMed: 18724357]

Jones JD, Dangl JL. The plant immune system. Nature. 2006; 444:323–329. [PubMed: 17108957]

Kawai T, Takahashi K, Sato S, Coban C, Kumar H, Kato H, Ishii KJ, Takeuchi O, Akira S. IPS-1, an adaptor triggering RIG-I- and Mda5-mediated type I interferon induction. Nat Immunol. 2005; 6:981–988. [PubMed: 16127453]

Kustermans G, El Benna J, Piette J, Legrand-Poels S. Perturbation of actin dynamics induces NF-kappaB activation in myelomonocytic cells through an NADPH oxidase-dependent pathway. Biochem J. 2005; 387:531–540. [PubMed: 15535802]

Lee CC, Kuo CJ, Ko TP, Hsu MF, Tsui YC, Chang SC, Yang S, Chen SJ, Chen HC, Hsu MC, et al. Structural basis of inhibition specificities of 3C and 3C-like proteases by zinc-coordinating and peptidomimetic compounds. J Biol Chem. 2009; 284:7646–7655. [PubMed: 19144641]

Legrand-Poels S, Kustermans G, Bex F, Kremmer E, Kufer TA, Piette J. Modulation of Nod2-dependent NF-kappaB signaling by the actin cytoskeleton. J Cell Sci. 2007; 120:1299–1310. [PubMed: 17356065]

Moser TS, Jones RG, Thompson CB, Coyne CB, Cherry S. A kinome RNAi screen identified AMPK as promoting poxvirus entry through the control of actin dynamics. PLoS Pathog. 2010; 6:e1000954. [PubMed: 20585561]

Mukherjee A, Morosky SA, Delorme-Axford E, Dybdahl-Sissoko N, Oberste MS, Wang T, Coyne CB. The Coxsackievirus B 3C Protease Cleaves MAVS and TRIF to Attenuate Host Type I Interferon and Apoptotic Signaling. PLoS Pathog. 2011; 7:e1001311. [PubMed: 21436888]

Mukherjee A, Morosky SA, Shen L, Weber CR, Turner JR, Kim KS, Wang T, Coyne CB. Retinoic acid-induced gene-1 (RIG-I) associates with the actin cytoskeleton via caspase activation and recruitment domain-dependent interactions. J Biol Chem. 2009; 284:6486–6494. [PubMed: 19122199]

Nemeth ZH, Deitch EA, Davidson MT, Szabo C, Vizi ES, Hasko G. Disruption of the actin cytoskeleton results in nuclear factor-kappaB activation and inflammatory mediator production in cultured human intestinal epithelial cells. J Cell Physiol. 2004; 200:71–81. [PubMed: 15137059]

Nolan K, Lacoste J, Parsons JT. Regulated expression of focal adhesion kinase-related nonkinase, the autonomously expressed C-terminal domain of focal adhesion kinase. Mol Cell Biol. 1999; 19:6120–6129. [PubMed: 10454559]

Onoguchi K, Onomoto K, Takamatsu S, Jogi M, Takemura A, Morimoto S, Julkunen I, Namiki H, Yoneyama M, Fujita T. Virus-infection or 5'ppp-RNA activates antiviral signal through redistribution of IPS-1 mediated by MFN1. PLoS Pathog. 2010; 6:e1001012. [PubMed: 20661427]

Richardson A, Parsons T. A mechanism for regulation of the adhesion-associated proteintyrosine kinase pp125FAK. Nature. 1996; 380:538–540. [PubMed: 8606775]

Schaller MD. Cellular functions of FAK kinases: insight into molecular mechanisms and novel functions. J Cell Sci. 2010; 123:1007–1013. [PubMed: 20332118]

Seth RB, Sun L, Ea CK, Chen ZJ. Identification and characterization of MAVS, a mitochondrial antiviral signaling protein that activates NF-kappaB and IRF 3. Cell. 2005; 122:669–682. [PubMed: 16125763]

Shen TL, Park AY, Alcaraz A, Peng X, Jang I, Koni P, Flavell RA, Gu H, Guan JL. Conditional knockout of focal adhesion kinase in endothelial cells reveals its role in angiogenesis and vascular development in late embryogenesis. J Cell Biol. 2005; 169:941–952. [PubMed: 15967814]

Tian M, Chaudhry F, Ruzicka DR, Meagher RB, Staiger CJ, Day B. Arabidopsis actin-depolymerizing factor AtADF4 mediates defense signal transduction triggered by the Pseudomonas syringae effector AvrPphB. Plant Physiol. 2009; 150:815–824. [PubMed: 19346440]

Wang W, Wen Y, Berkey R, Xiao S. Specific targeting of the Arabidopsis resistance protein RPW8.2 to the interfacial membrane encasing the fungal Haustorium renders broad-spectrum resistance to powdery mildew. Plant Cell. 2009; 21:2898–2913. [PubMed: 19749153]

Xu LG, Wang YY, Han KJ, Li LY, Zhai Z, Shu HB. VISA is an adapter protein required for virus-triggered IFN-beta signaling. Mol Cell. 2005; 19:727–740. [PubMed: 16153868]

Zhang HM, Keledjian KM, Rao JN, Zou T, Liu L, Marasa BS, Wang SR, Ru L, Strauch ED, Wang JY. Induced focal adhesion kinase expression suppresses apoptosis by activating NF-kappaB signaling in intestinal epithelial cells. Am J Physiol Cell Physiol. 2006; 290:C1310–1320. [PubMed: 16354757]

Zhu, J.; Coyne, CB.; Sarkar, SN. PKC alpha regulates Sendai virus-mediated interferon induction through HDAC6 and beta-catenin.. The EMBO journal. 2011.

Highlights

- FAK deficiency enhances RNA virus replication and impairs NF-κB and IFNβ induction
- FAK is involved in MAVS-mediated antiviral signaling
- FAK interacts with MAVS following virus infection and redistributes to mitochondria
- An enterovirus encoded protease cleaves FAK to attenuate antiviral signaling

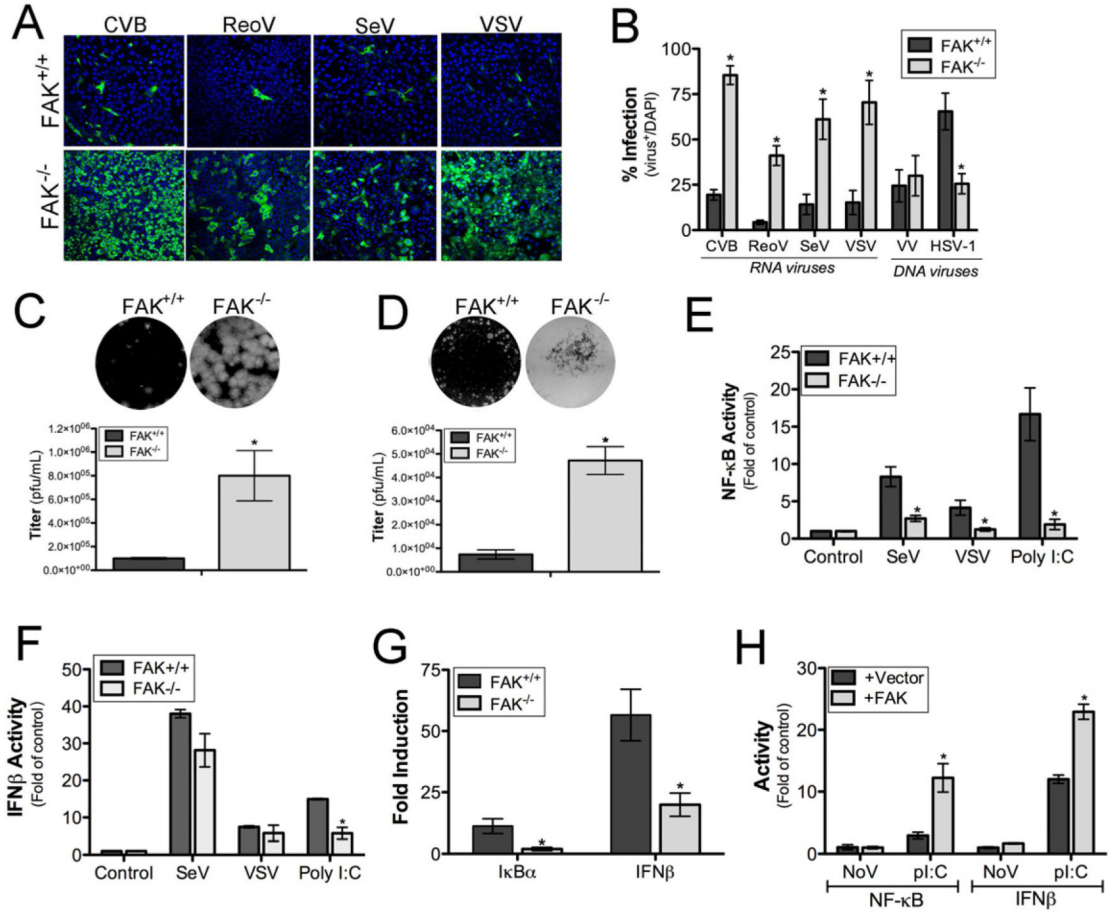

Figure 1. FAK Depletion Enhances RNA Virus Replication and Attenuates Antiviral Signaling

(A), FAK$^{+/+}$ or FAK$^{-/-}$ MEFs were infected with CVB (MOI=1), ReoV (MOI=5), SeV (10 HAU/mL), or VSV (MOI=0.1) for 16 hr. Cells were fixed and stained for markers of virus infection (CVB [VP1], ReoV [polyclonal antisera], SeV [C protein]) or assessed for GFP expression (VSV-GFP). Blue, DAPI-stained nuclei. **(B)**, FAK$^{+/+}$ or FAK$^{-/-}$ MEFs were infected with CVB (MOI=1), ReoV (MOI=5), SeV (10 HAU/mL), VSV (MOI=0.1), VV (MOI=10), or HSV-1 (MOI=5) for 16 hr. Following infection, cells were fixed and stained for markers of virus infection (CVB [VP1], ReoV [polyclonal antisera], SeV [C protein]) or assessed for GFP expression (VSV-GFP, VV-GFP, HSV-1-GFP). Level of infection was calculated based on the percent of virus-infected cells over total cells, as assessed by DAPI-staining. **(C, D)**, Plaque assays for VSV performed using FAK$^{+/+}$ and FAK$^{-/-}$ MEFs (C) or CVB in HeLa cells on lysates harvested from FAK$^{+/+}$ or FAK$^{-/-}$ MEFs. Top, representative wells from the 10^{-6} dilution of virus are shown. Bottom, quantification of viral titers. **(E, F)**, Luciferase assays from FAK$^{+/+}$ or FAK$^{-/-}$ MEFs transfected with NF-κB (C) or IFNβ (D) promoted luciferase constructs and infected with SeV (20 HAU/mL) or VSV (MOI=0.5) or transfected with poly(I:C) (100 ng) for 16 h following transfection (24 hr). **(G)**, FAK$^{+/+}$ or FAK$^{-/-}$ MEFs were transfected with 100 ng poly(I:C). Total RNA was extracted ~ 24 hr post-transfection and analyzed by quantitative RT–PCR for IkBα (left) and IFN-β (right) mRNA. **(H)**, Luciferase assays from FAK$^{-/-}$ MEFs transfected with NF-κB or IFNβ promoted luciferase constructs and either vector or FAK. Following transfection (24 hr), cells were transfected with poly(I:C) (100 ng) for 16 hr and luciferase activity measured. Data in (B-H) are shown as mean ± standard deviation. Asterisks indicate *P*-values of ≤ 0.05.

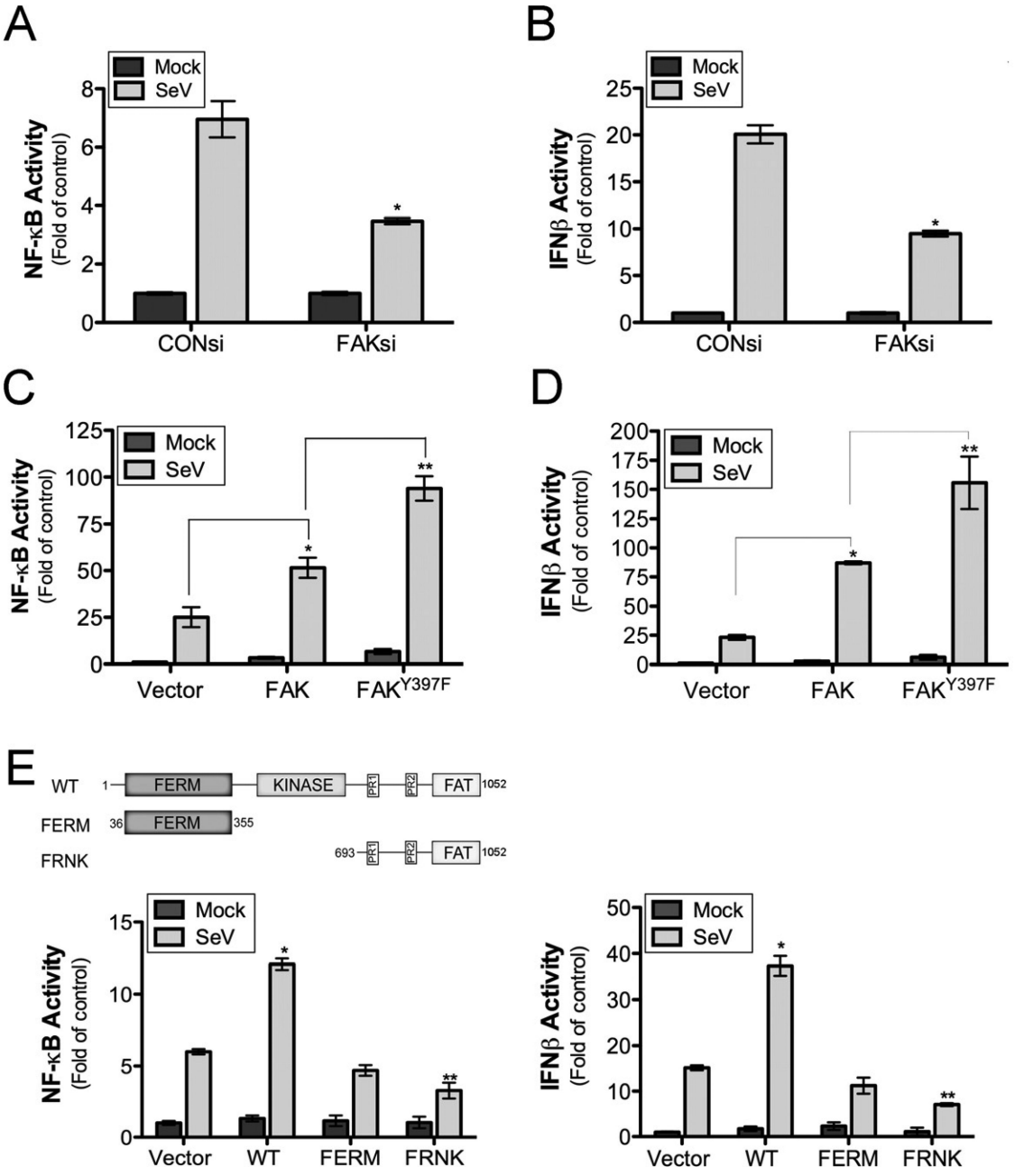

Figure 2. FAK Contributes to Antiviral Signaling via a Kinase-independent Mechanism

(A, B), Luciferase assays from HEK293 cells transfected with NF-κB (A) or IFNβ (B) promoted luciferase constructs following by transfection with control (CON) or FAK siRNAs. Following transfection (24 hr), cells were infected with SeV (25 HAU/mL) or PBS (mock) for 18 hr and luciferase activity measured. **(C, D)**, Luciferase assays from HEK293 cells transfected with NF-κB (C) or IFNβ (D) promoted luciferase constructs and either vector control, wild-type FAK, or a kinase-defective FAK mutant (Y397F). Following transfection (24 hr), cells were infected with SeV (25 HAU/mL) or PBS (mock) for 18 hr and luciferase activity measured. **(E)**, Luciferase assays from HEK293 cells transfected with NF-κB (left) or IFNβ (right) promoted luciferase constructs and vector control, wild-type FAK, and either the FAK FERM domain or FRNK. Following transfection (24 hr), cells were infected with SeV (25 HAU/mL) or PBS (mock) for 18 hr and luciferase activity measured. Top, schematic of FAK constructs. Data are shown as mean ± standard deviation. Asterisks indicate *P*-values of ≤ 0.05.

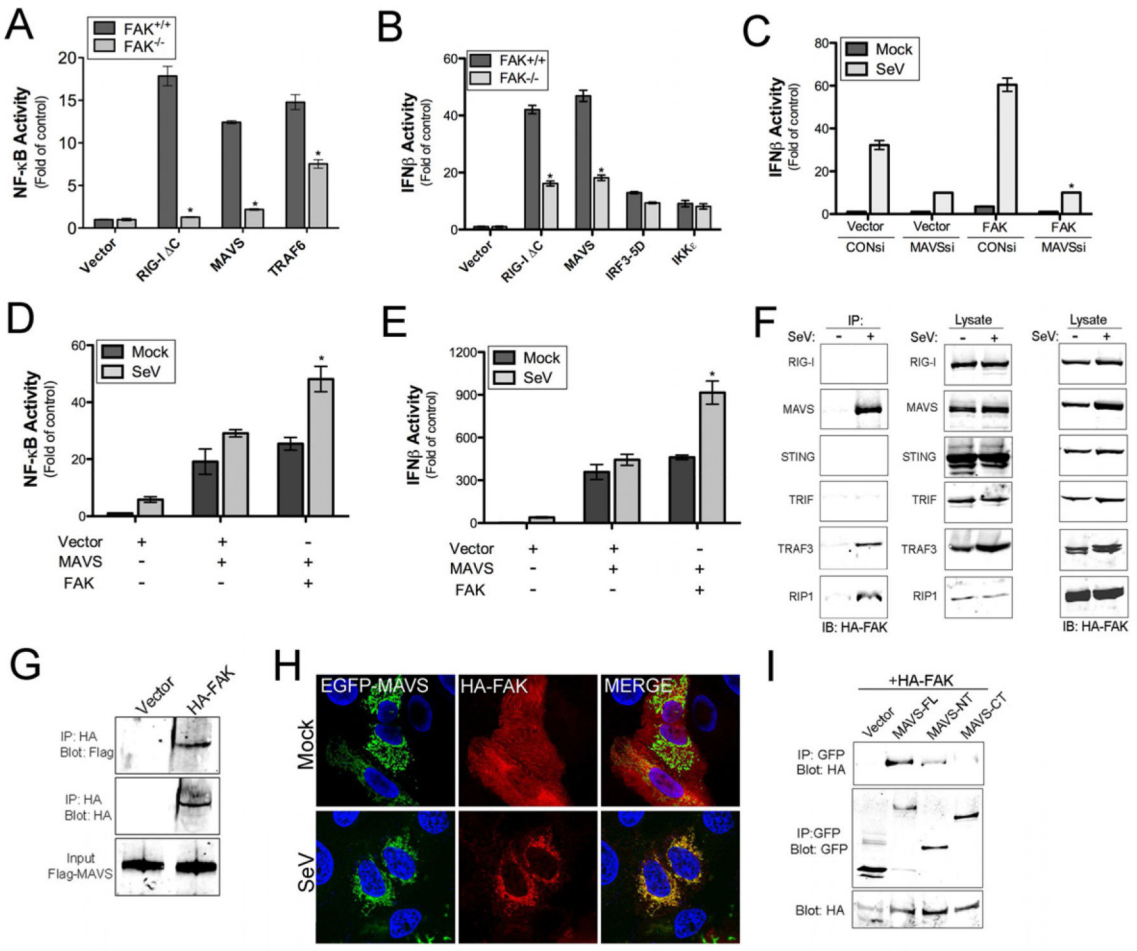

Figure 3. FAK Interacts with MAVS and other Components of RLR Signaling in Response to Virus Infection

(A, B), Luciferase assays from FAK$^{+/+}$ or FAK$^{-/-}$ MEFs transfected with NF-κB (A) or IFNβ (B) promoted luciferase constructs and the indicated plasmids 24 hr post-transfection. **(C, D)**, Luciferase assays from HEK293 cells transfected with NF-κB (C) or IFNβ (D) promoted luciferase constructs and either vector, MAVS, or FAK alone or in combination. Cells were infected with SeV (25 HAU/mL) or PBS (mock) for 18 hr following transfection (24 hr) and luciferase activity measured. **(E)**, Luciferase assay from HEK293 cells transfected with an IFNβ promoted luciferase construct and either control (CON) or MAVS siRNA. Cells were infected with SeV (25 HAU/mL) or PBS (mock) for 18 hr following transfection (48 hr) and luciferase activity measured. **(F)**, Co-immunoprecipitation studies from HEK293 cells transfected with HA-FAK and the indicated constructs. Following transfection (48 hr), cells were infected for 18 hr with SeV (10 HAU/mL) and lysed. Lysates were subject to immunoprecipitation with antibodies directed against GFP (RIG-I, MAVS, STING, TRIF) or Flag (TRAF3, RIP1). Following washing, lysates were immunoblotted for HA-FAK (left panel) and GFP or Flag (middle panel). In parallel, lysates were immunoblotted for HA-FAK to control for the level of expression (right panel). **(G)**, *In vitro* binding assays from HEK293 cells transfected with HA-FAK. Following transfection (24 hr), cells were infected for 18 hr with SeV (10 HAU/mL) and lysed. Lysates were subject to immunoprecipitation with anti-HA antibody. Following washing, recombinant Flag-MAVS was added to immunoprecipitates. Following washing, immunoprecipitates were immunoblotted for Flag-MAVS (top) and HA-FAK (middle). In parallel, lysates were immunoblotted for Flag-MAVS to control for the level of expression (bottom). **(H)**, U2OS cells were transfected with EGFP-MAVS and HA-FAK and infected with SeV (25 HAU/mL) for 18 hr. Following infection, cells were fixed, stained for FAK (HA, red), and imaged by confocal microscopy. Blue, DAPI-stained nuclei. **(I)**, Co-immunoprecipitation studies using HEK293 cells transfected with HA-FAK and either full-length MAVS (MAVS-FL) or N-

terminal (MAVS-NT) or C-terminal (MAVS-CT) fragments of MAVS. Following transfection (48 h), cells were infected for 18 hr with SeV (10 HAU/mL) and lysed. Lysates were subject to immunoprecipitation with antibodies directed against GFP and immunoblotted for HA-FAK (top panel) or GFP (middle panel). In parallel, lysates were immunoblotted for HA-FAK to control for the level of expression (bottom panel). Data in (A -E) are shown as mean ± standard deviation. Asterisks indicate *P*-values of ≤ 0.05.

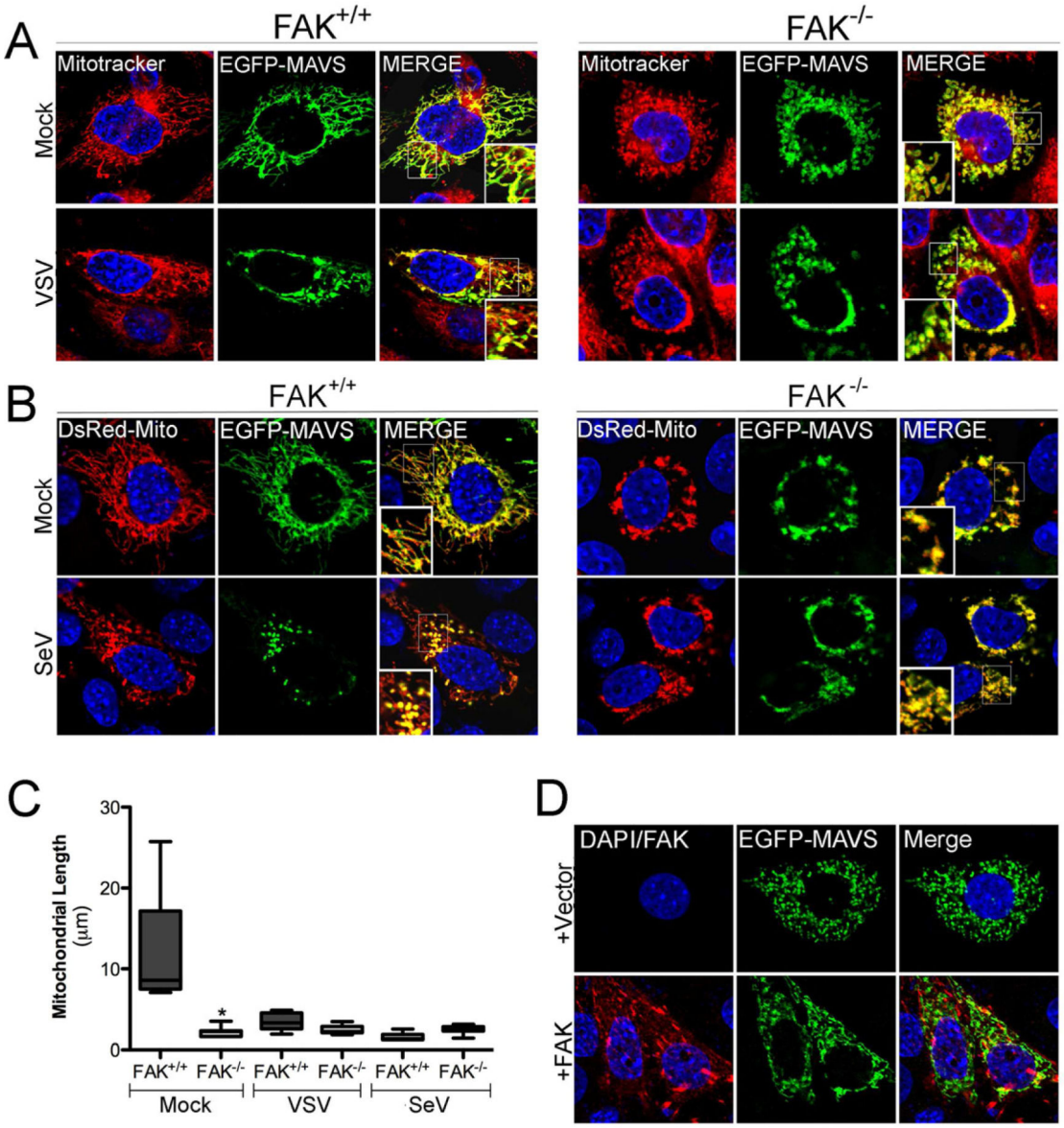

Figure 4. FAK Relocalizes to the Mitochondrial Membrane in Response to Virus Infection and Facilitates MAVS localization

(A), FAK$^{+/+}$ or FAK$^{-/-}$ MEFs were transfected with EGFP-MAVS and 24 hr following transfection, infected with VSV (MOI=1) for 6 hr. Following infection, cells were incubated with Mitotracker (red), fixed, and imaged by confocal microscopy. Blue, DAPI-stained nuclei. **(B)**, FAK$^{+/+}$ or FAK$^{-/-}$ MEFs were transfected with EGFP-MAVS and DsRed-Mito and 24 hr following transfection, infected with SeV (100 HAU/mL) for 16 hr. Following infection, cells were fixed and imaged by confocal microscopy. Blue, DAPI-stained nuclei. **(C)**, Quantification of MAVS-associated mitochondrial length from cells shown in (A) and (B). Data are representative of a minimum of 100 individual mitochondrial filaments from at least 30 cells from three independent experiments. **(D)**, FAK$^{-/-}$ MEFs were transfected with vector (top row) or wild-type FAK (bottom row) and EGFP-MAVS. Following transfection (48 hr), cells were fixed, stained for FAK (in red), and imaged by confocal microscopy. Data in (C) are shown as mean ± standard deviation. Asterisks indicate *P*-values of ≤ 0.05.

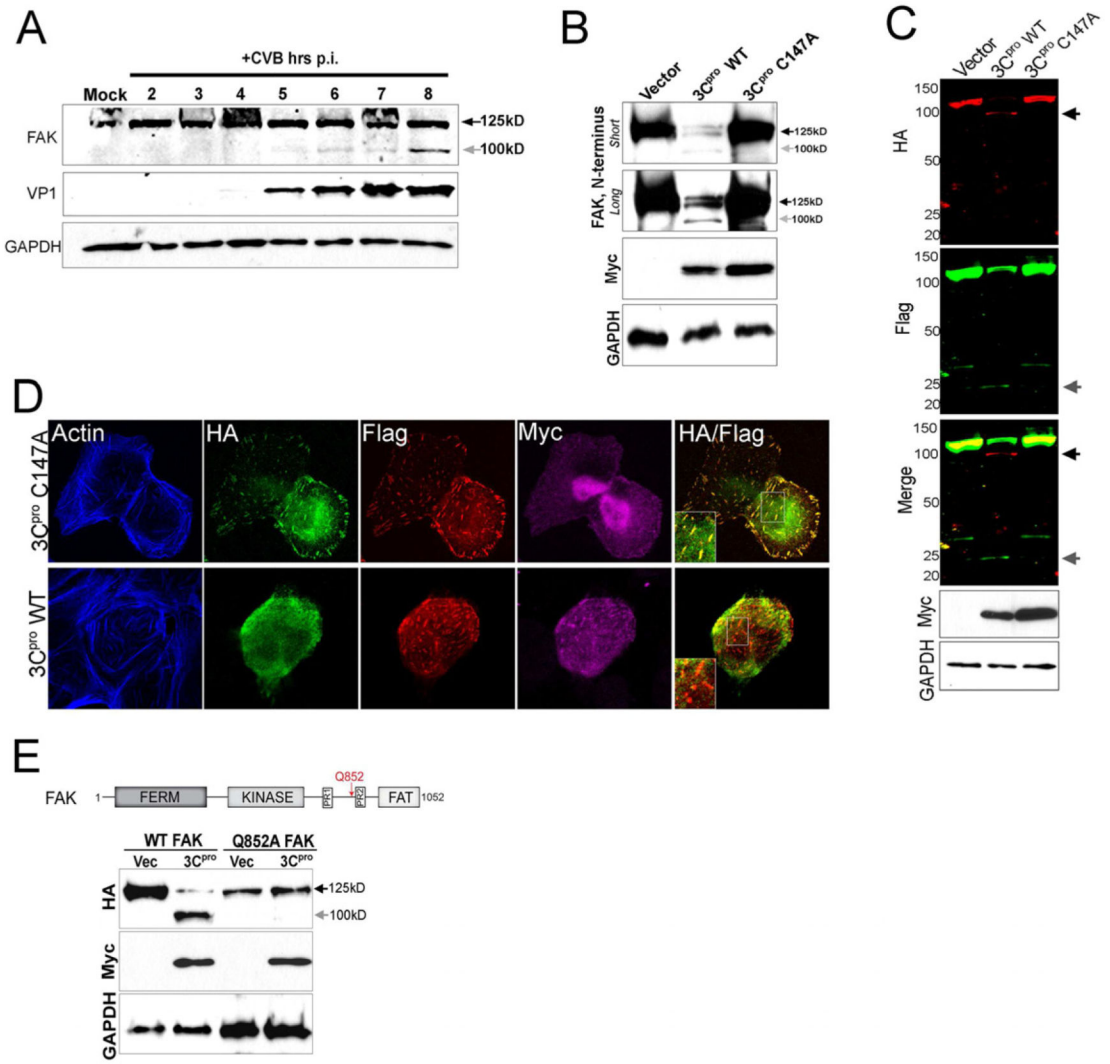

Figure 5. CVB Infection Induces FAK Cleavage by 3C^{pro}

(A), Immunoblot analysis of FAK (using an antibody directed against the N-terminus, top) and VP1 (middle) in Caco-2 cells infected with CVB for the times shown. Grey arrow denotes a CVB-induced cleavage fragment of ~ 100 kD. Immunoblotting for GAPDH (bottom) is included as a loading control. **(B)**, Immunoblot analysis for endogenous FAK using an antibody directed against the N-terminus in cells transfected with vector or Myc-tagged wild-type (WT) or C147A 3C^{pro}. Immunoblotting for GAPDH (bottom) is included as a loading control. **(C)**, Dual-color immunoblot analysis using a LI-COR Odyssey infrared imaging system and antibodies specific for HA (700nm, red) and Flag (800nm, green) in HEK293 cells transfected with vector, Myc-3C^{pro} wild-type or C147A, and HA-FAK-Flag. Black arrows denote full-length and cleavage fragments. An overlay of both channels is shown below (with yellow indicating overlapping signals). **(D)**, Confocal microscopy from U2OS cells transfected with Myc-wild-type (WT) or mutant (C147A) 3C^{pro} and HA-FAK-Flag. Cells were fixed 48 h following transfection and stained for HA (green), Flag (red), Myc (purple), and actin (blue). Areas of colocalization appear as yellow. **(E)**, Top, schematic of full-length FAK indicating the location of the FERM, kinase, and FAT domains, two proline-rich regions, and the location of a 3C^{pro}-mediated cleavage site at position Q852 (red arrow). Bottom, immunoblot analysis for HA-FAK (top) and Myc (bottom) in cells transfected with either WT or mutant FAK (Q852A) and vector control or Myc-WT 3C^{pro}. Grey arrow denotes the presence of a ~ 100 kD cleavage fragment.

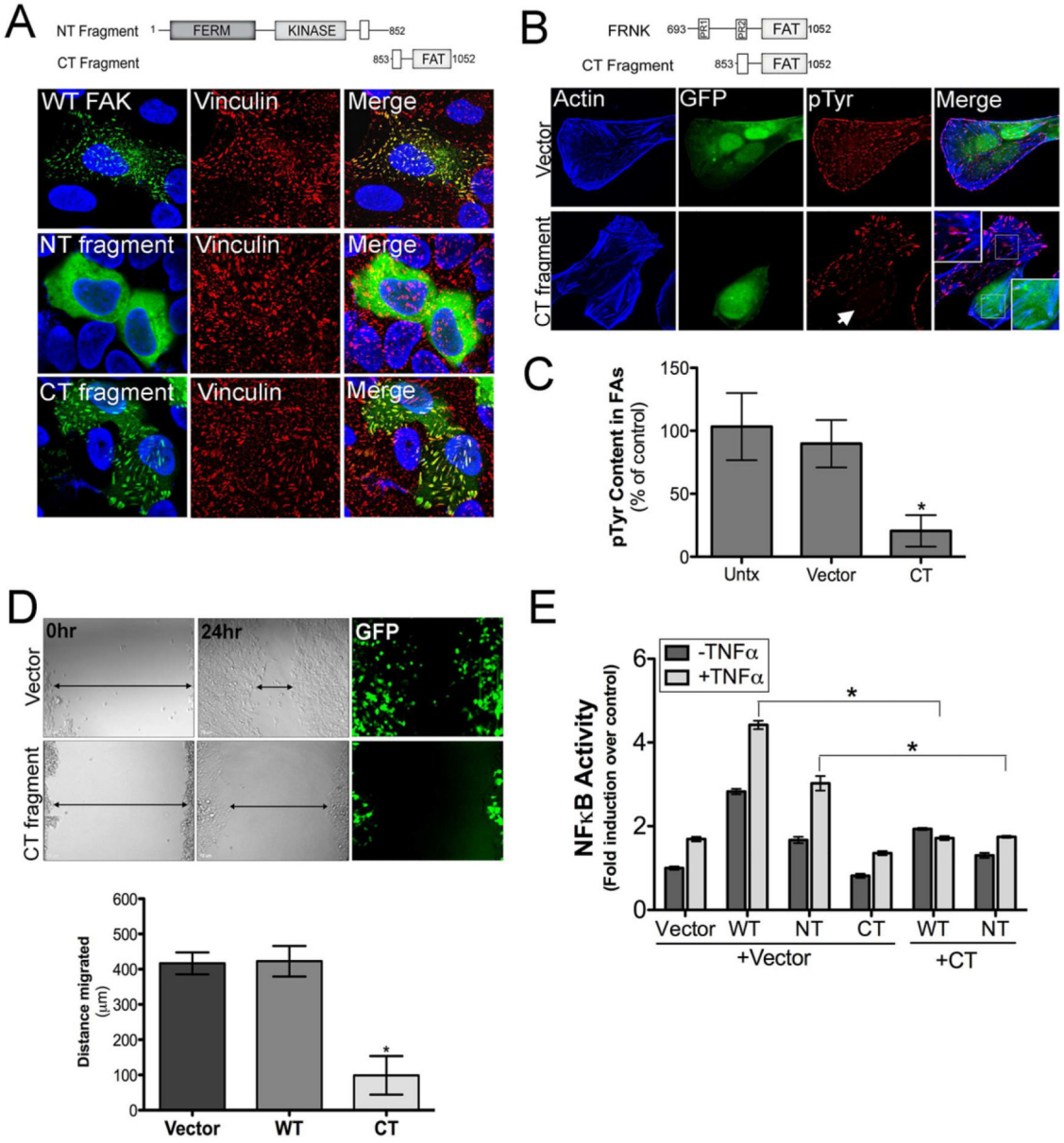

Figure 6. The C-terminal Cleavage Fragment of FAK Functions as an FRNK-like Polypeptide

(A), Top, schematic of N-terminal (NT) or C-terminal (CT) $3C^{pro}$ cleavage fragments of FAK. Bottom, confocal microscopy of U2OS cells transfected with wild-type FAK (and stained for HA, green) or EGFP-fused NT and CT fragments. Vinculin staining of FAs is shown in red. **(B)**, Top, schematic of FRNK and the $3C^{pro}$ generated C-terminal FAK cleavage fragment. Bottom, confocal micrographs of U2OS cells transfected with vector control or EGFP-CT fragment and stained for actin (blue) and phosphorylated tyrosine residues (pTyr) (red). **(C)**, Quantification of pTyr content in FAs from images shown in (B). **(D)**, Top, differential interference contrast (DIC) images and GFP fluorescence from wound healing assays in HEK293 cells transfected with vector control or with the CT fragment of FAK at 0hr and 24hr post-wounding. Black arrows denotes general width of the wound. Bottom, Quantification of the distance migrated (in μm between 0hr and 24hr following wound induction) in cells transfected with vector control, WT FAK, or the CT fragment of FAK. **(E)**, Luciferase assays from U2OS cells transfected with a NF-κB promoted luciferase construct and either vector control, WT FAK, NT-, or CT-fragments of FAK alone or in combination. Forty-eight hours post-transfection, cells were stimulated with TNFα (1ng) for 60min and lysates

collected for luciferase assays. Data in (C-E) are presented as mean ± standard deviation from experiments performed in triplicate a minimum of three times, *p<0.05.

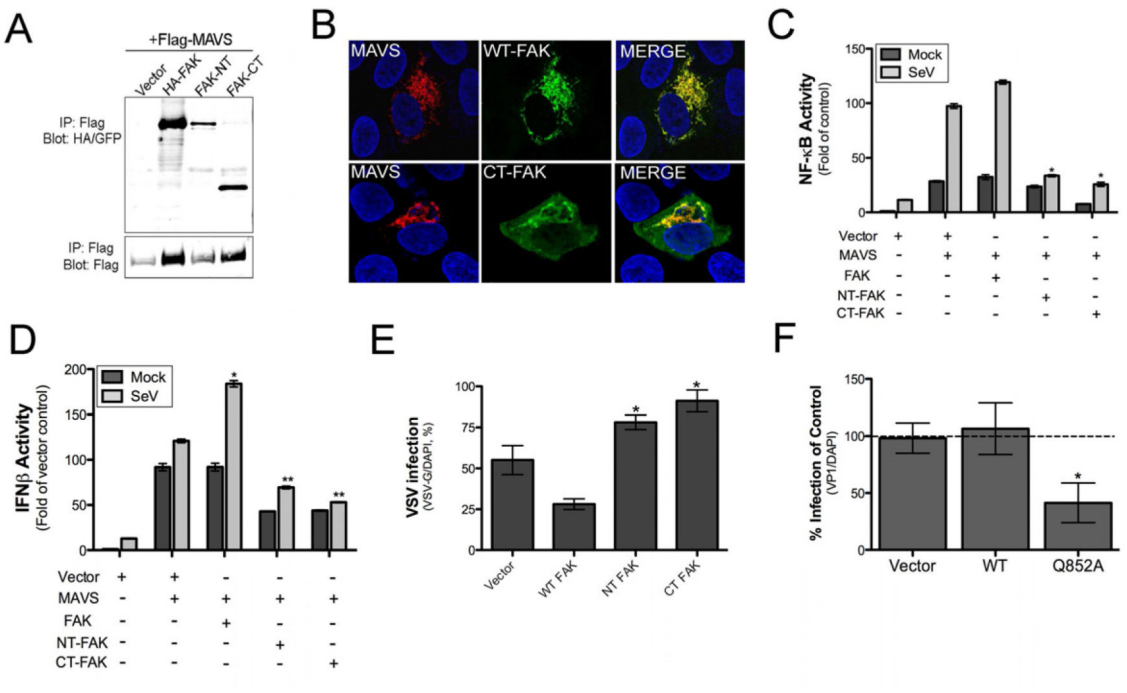

Figure 7. 3C^{pro} Cleavage Fragments of FAK Bind MAVS and Inhibit MAVS-mediated Antiviral Signaling

(A), Co-immunoprecipitation studies using HEK293 cells transfected with Flag-MAVS and either full-length FAK (HA-FAK) or N-terminal (FAK-NT) or C-terminal (FAK-CT) fragments of FAK. Following transfection (48 hr), cells were infected for 18 hr with SeV (10 HAU/mL) and lysed. Lysates were subjected to immunoprecipitation with anti-Flag antibody and immunoblotted for HA-FAK (top panel) or Flag (bottom panel). **(B)**, U2OS cells were transfected with Flag-MAVS and either WT (HA-FAK) or CT-FAK (bottom) and infected with SeV (25 HAU/mL) or PBS (mock) for 18 hr. Following infection, cells were fixed, stained for MAVS (Flag, red), FAK (HA, green, top), or both proteins, and imaged by confocal microscopy. Blue, DAPI-stained nuclei. **(C, D)**, Luciferase assays from HEK293 cells transfected with NF-κB (C) or IFNβ (D) promoted luciferase construct and either vector control, MAVS, WT FAK, NT-, or CT-fragments of FAK alone or in combination. Twenty-four hr post-transfection, cells were infected with SeV (20 HAU/mL) or PBS (mock) and luciferase activity determined. **(E)**, Quantification of VSV infection (based on VSV-G staining and expressed as percent infection) in U2OS cells transfected with vector control, WT, NT, or CT FAK constructs. **(F)**, Quantification of CVB infection (based on VP1 staining and expressed as a percent of vector control) in U2OS cells transfected with vector control, WT FAK, or Q852A FAK. In (C-F) data are presented as mean ± standard deviation from experiments performed in triplicate a minimum of three times. *, $P < 0.05$.